Dear Lachlan,

Congratulations on Academic Excellence for Study Period 2, 2022.

On behalf of the University, I would like to personally congratulate you on the excellent academic results you achieved in Study Period 2, 2022 toward your program of study with the University.

- ELC205 Control Systems - DN
- ENG304 Eng Research Methodology - HD
- MEC303 Computational Mechanics - HD
- MEC336 Engineering System Design - HD

Academic Excellence letters are sent out to students that achieve a GPA of 6.75 or above for a study period, and therefore is received by only a very small percentage of students.

This achievement undoubtedly reflects many long hours of intense study on your part, which I commend you for.

Once again, congratulations on your excellent results, and best wishes for continued success in your studies at the University of the Sunshine Coast.

Yours sincerely,

Professor Tim Wess
Deputy Vice-Chancellor (Academic)

Lachlan Wensley - Feedback for Production Engineering Task 1B

I would like to extend my sincere appreciation for the outstanding report you have submitted. It is evident that you have invested significant effort in crafting a clear and cohesive document. The logical flow of your report is easy to follow, and the solution you have presented is indeed correct. I must commend you on the exceptional quality of your work. Your meticulous attention to detail and remarkable ability to convey complex information in a concise and understandable manner are truly impressive. Your report is a testament to your professionalism and expertise in the subject matter. While your report is already exceptional, I believe there is potential for further improvement in certain areas. Fine-tuning specific sections to enhance clarity and providing additional supporting evidence in certain areas could elevate the overall impact of your work. However, it is important to note that these suggestions do not diminish the fact that your work is already of an exceptional standard. Congratulations on your outstanding achievement! Your unwavering dedication and commitment are evident in the high caliber of your report. I am genuinely excited to witness your future contributions and the remarkable work you will continue to produce. Please keep up the excellent work, and know that your efforts are truly valued and appreciated.

- Rezwanul Haque

Design and Simulation of a Magnetorheological Brake

School of Science, Technology and Engineering, University of the Sunshine Coast

Student Name: Lachlan Wensley

Student ID# 1109326

Academic Advisor: Tongfei Tian

Chapter 2 Literature Review

2.1 Chapter Introduction

This chapter focusses on the mechanical components in automotive vehicles, specifically discussing hydraulic brakes and introducing electrorheological (ER) and magnetorheological (MR) smart fluids as potential alternatives. Hydraulic brakes, the conventional braking method, play a crucial role in regulating speed and deceleration, however, exhibit limitations such as driver error, delayed response time and noise. The subsequent discussion delves into ER and MR smart fluids, examining their characteristics, applications, and advantages. The properties and potential of these fluids is compared, and highlights MR fluids as a superior choice due to their higher yield stress, greater energy dissipation, and reliability. The chapter also explores the applications of MR fluids in the automotive industry such as damping and vibration control, semi-active shock absorbers, and electrically engaged clutches. The following chapter discusses the application of MR fluid in brake designs showing promising potential for enhancing braking performance and reducing response time.

2.2 Mechanical Components in Automotive Vehicles

To attain maximum efficiency in vehicle engines, it is necessary to increase the ratio of the work generated by the engine to the energy consumed. Thorough research on the electronic controls of engines resulted in major improvements from carburettor fed engines to modern engines with electronic fuel injection. This advanced electronic module determines the optimal fuel delivery to the engine by analysing factors such as accelerator position, engine speed and temperature. Leen & Heffernan (2002) noted that relying solely on mechanical components precludes the integration of multiple electronic systems in vehicles, emphasising the importance of electric alternatives for replacing remaining mechanical parts. Not only do such replacements offer economic and environmental benefits but can also lead to significant enhancements in vehicle performance.

2.3 Hydraulic Brakes

As explained in the previous section, the braking system in automotive vehicles have the potential for the mechanical components to be replaced with electrical components. Hydraulic disk brakes are considered most popular and therefore will be considered the conventional braking method in this thesis. A brake is a mechanism that hinders the motion of a moving system by absorbing its energy through friction. The conversion of kinetic energy into thermal energy is achieved through dry friction, and the heat generated is dissipated into the environment (Sau et. al. 2022). In the case of an automobile, the braking system is responsible for regulating the speed, smoothness, and straightness of the car's deceleration. A brake disc plate is attached to and rotates with the wheel. The brake pedal of a car is connected to a master cylinder, which contains hydraulic fluid that transfers the force to the brake pads inside each wheel assembly. Two brake pads are housed inside a calliper, which is mounted on the knuckle connected to the chassis. When the driver applies the brakes, the hydraulic fluid in the master cylinder is pressurised and transported via brake lines to the calliper. The pressurised hydraulic fluid then pushes the piston, which squeezes the brake pads against the rotor. The friction between the brake pads and disc produces a braking torque on the wheel, which slows down the car through the resulting friction between the tire and road surface (Thakur 2018). Figure 2.1 shows an example of a hydraulic disc brake assembly comprising of a ventilated disc, a sliding calliper with a single piston, and two brake pads.

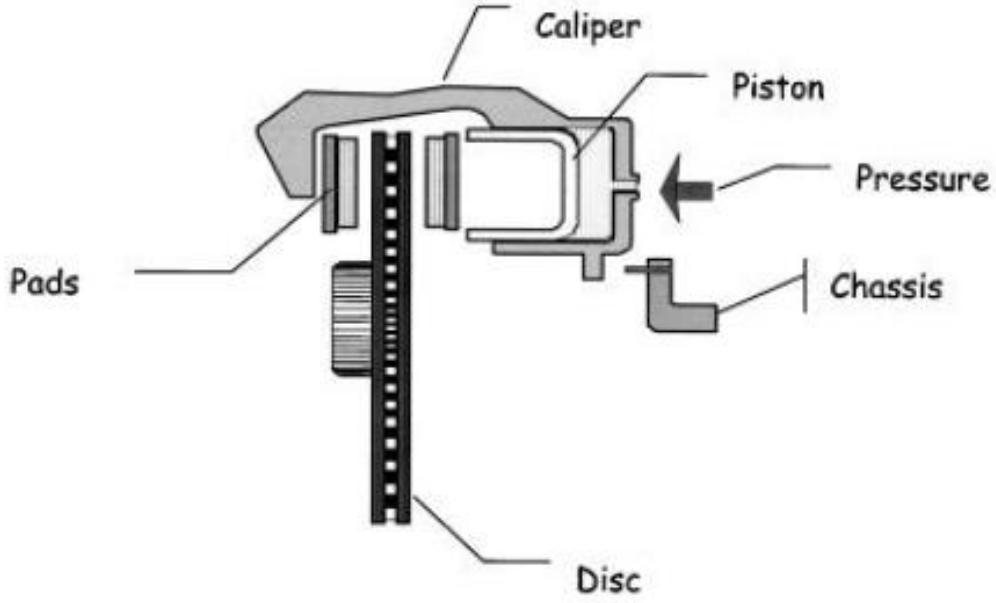

Figure 2.1 Schematic of hydraulic disc brake (Thakur 2018).

Falcão da Luz (2002) states that driver error plays a big role in optimal braking efficiency where the incorrect brake pressure may be applied resulting in the wheels locking, further losing steering control. The purpose of anti-lock braking system (ABS) is to identify instances when a wheel has locked and regulate the brake pressure accordingly. However, since braking systems continue to rely mostly on hydraulic mechanisms, achieving this goal necessitates the use of valves for adjusting the brake pressure. This slows down the system's response, negatively impacts the braking distance, and adds weight from additional components (Falcão da Luz 2002).

Park et. al. (2006) further explains the limitation of hydraulic brakes in the perspective of driver error. It is shown that from the moment the driver applies pressure to the brake pedal, to the moment the pressure is transmitted to the brake pads there is a 200-300ms delay. Falcão da Luz (2002) develops further on this, outlining the significant increase in braking distance. When a car is travelling at 120km/h, it travels 6.5 metres before the effects of braking are applied to the vehicle. When travelling at 100km/h this length accounts for 12% of the typical braking distance at that speed.

A paper by Dakhil et. al. (2014) conducted a study aiming to enhance the performance of disk brakes through the utilisation of finite element analysis. Their research focused on

evaluating the braking capabilities of disk brakes when subjected to extreme braking conditions. The paper highlights a further drawback of conventional hydraulic disk brakes due to its exposure to external elements such as oil and grease that can affect the braking performance or damage the disk. The number of mechanical components in hydraulic brakes also make the system more prone to failure due to fluid leaks or ageing of brake fluid.

Joe et. al. (2007) investigated the occurrence of hydraulic disk brake instability caused by friction-induced vibration. While a significant amount of research has traditionally emphasised braking power and reliability in brake systems, the aspects of noise and vibration has often been given less importance. The noise during braking, also known as 'squeal', is caused by the modal coupling due to friction forces. Disk brake noise is a problem that continues to confront automobile manufacturers, with customer dissatisfaction resulting in possible loss of future business. The study shows that factors such as the friction coefficient, lining stiffness, length of the pads, thickness of the lining, Young's modulus and the mass of the system all play a role in the stability of the braking system and the resultant braking 'squeal'.

As indicated, conventional hydraulic brakes whilst having various advantages also have disadvantages that have the potential to be overcome with electric components. This warrants the investigation into smart materials that could be implemented into braking system designs.

2.4 Electrorheological and Magnetorheological Smart Fluids

In section 2.1, the drawbacks of traditional hydraulic brakes are examined, along with potential solutions involving electric systems and smart materials. To this end, a comprehensive review of electrorheological (ER) and magnetorheological (MR) smart fluids was conducted to gain insight into the characteristics and constraints of each substance. Both types of fluids possess the ability to alter their viscosities through the application of an electric or magnetic field respectively (Jolly, Carlson & Muñoz 1996).

Hao (2001) describes the basic structure of ER fluid which consists of a suspension of submicron-sized particles in a non-conducting liquid. When the electric field is applied to the fluid, the particles align along the field lines, leading to the formation of chains and clusters that increase the fluids viscosity and stiffness. The extent of this variation relies on several

factors, including the intensity of the electric field employed, the concentration of particles, and the dimensions and configuration of the particles involved. ER fluids have been studied for their applications in various areas such as vibration control, robotics, and microfluidics.

Stanway, Sproston & El-Wahed (1996) conducts a survey on the applications of electro-rheological fluids in vibration control. In vibration control, electro-rheological fluids can be used to minimise the vibration amplitudes of machines, structures, or vehicles. This is done by changing the fluids stiffness and damping properties in response to the frequency and amplitude of the vibration. This then absorbs and dissipates the energy of the vibration, reducing the amplitude. Sturk, Wu & Wong (2007) suggested an ER damper-equipped high voltage supply unit and demonstrated its efficacy through a quarter car suspension system. More recently, Seung-Bok, Young-Min & Kum-Gil (2008) presented a specially designed cylindrical ER damper intended for use in passenger vehicles. They successfully demonstrated the effectiveness of controlling the damping force of the damper by incorporating a skyhook controller. Nguyen & Choi (2012) provide and analytical approach to the design of an ER damper tailored for vehicle suspension systems, emphasising stability and ride comfort. They incorporate the principles of Bingham rheological laws governing ER fluids, and present a design based on a quasi-static model as shown in Figure 2.2.

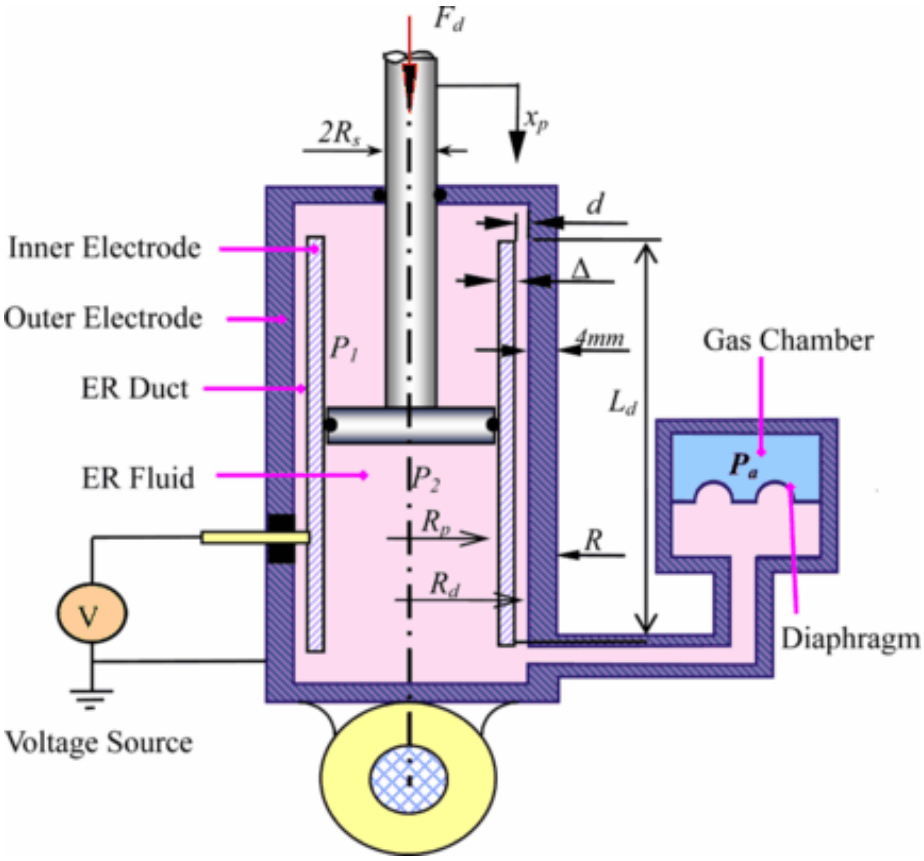

Figure 2.2 Schematic Configuration of an ER damper (Nguyen & Choi 2012)

Acerbi & Mingione (2002) investigates the use of a mathematical model to represent electro-rheological fluids. Based on the findings, it is indicated that when exposed to an electromagnetic field, these fluids have the capability to undergo significant alterations in their mechanical properties, including a viscosity variation of up to a factor of 1000. While ER fluids offer a great deal of promise for use in various engineering applications, their widespread adoption is still limited due to several challenges outlined by Stanway (2004). These challenges include the need to develop ER fluids that exhibit high stability, low hysteresis, and low power consumption. Moreover, the relatively high cost of ER fluids and the complexity involved in their manufacturing processes serve to restrict their commercial viability.

Raju & Varma (2017) discusses the behaviours of MR fluids. When no magnetic field is applied to MR fluids, they typically behave as Newtonian liquids. This means that the viscosity is independent of the shear rate. Although when a magnetic field is applied to the fluid, magnetic dipole and multipole moments are induced on each particle. The anisotropic forces between the particles promote the correct alignment and draws the particles into proximity of one another. Consequently, particle chains, columns, or intricate networks are created, which

impede the fluid's movement, leading to heightened viscosity of the MRF as shown in Figure 2.3. The energy necessary for the formation of these chain-like structures increases in proportion to the intensity of the applied field, resulting in a yield stress that is contingent upon the magnetic field. One of the key challenges faced with the use of MR fluids is being able to optimise its rheological properties. Gopinath & Sathishkumar (2021) show that research has been done on the effect various parameters such as particle size, particle concentration and carrier fluid viscosity have on the rheological properties of MR fluids and their effectiveness. Ahamed, Choi & Ferdaus (2018) conducted a study that further illustrates this, showing a decrease in performance efficiency over time with the sedimentation of iron particles in MR fluid shock absorbers and engine mounts. Further limitations show the effect of high temperatures on MR fluids and the ineffectiveness as a result.

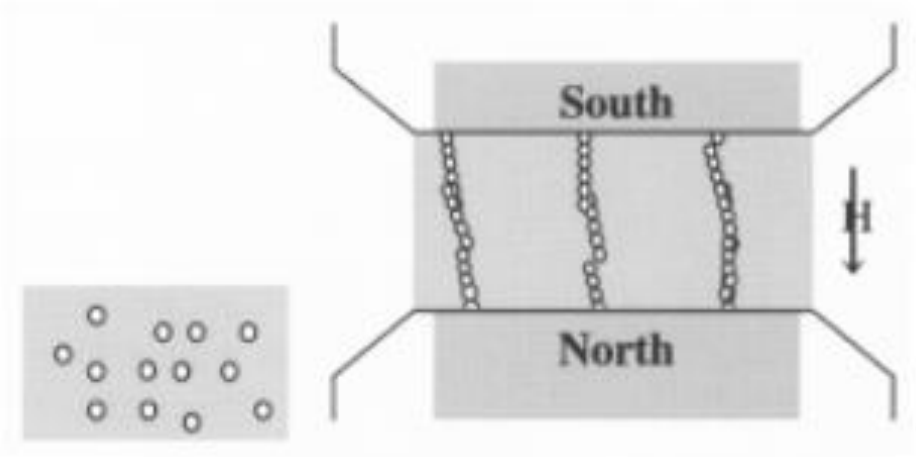

Figure 2.3 Magnetorheological Fluid Particle Alignment (Raju & Varma 2017)

Kumar et. al. (2019) reviews the applications of MR fluids and the major challenges that need to be mitigated when preparing and storing the material. MR fluids consist of three main components: magnetic particles, carrier fluid, and additives. In most cases, the magnetic particles employed are carbonyl iron, known for their exceptional magnetic permeability and saturation magnetisation. These particles possess a purity level of 99% due to their desirable properties. Spherical carbonyl iron particles are often used over fibre shaped particles due to the reduction on the effects of wear on the walls of the container or device that holds the MR fluid. Although Kumar et. al. (2019) does state that fibre shaped particles show a better yield stress and low viscosity when under no magnetic field compared to spherical particles. The concentration of the iron particles range from 20-40% with an average size of 4.25um.

Gopinath & Sathishkumar (2021) agrees with this paper and emphasised that particle size is an important factor as small sizes will not produce enough yield stress, while large particle sizes can cause friction and erosion issues. To ensure that there is no chemical interaction with the iron particles, the carrier fluid utilised is typically mineral oil, silicone oil, or other synthetic oils with low viscosities. In vibration control applications, silicone oil is commonly preferred due to its advantageous properties such as a high viscosity index, low friction characteristics, and high shear strength. Kumar et al (2019) provides further insight by explaining that additives, such as surfactants, are incorporated into the fluid. These additives serve the purpose of preventing agglomeration of magnetic particles or slowing down the rate of particle settling.

Before considering the use of either of these materials, it is crucial to have a comprehensive understanding of their individual characteristics. A comparison of their properties, from Lord Corporation, is presented in Table 2.1. This provides an overview of the materials and serves as a useful reference point for evaluating the advantages and disadvantages of each fluid.

Table 2.1 Magnetorheological versus Electrorheological Fluids

	MR FLUID	ER FLUID
Maximum. Yield Stress	50-100 kPA	2-5 kPa
Maximum. Field	250 kA/m	4 kV/m
Viscosity	0.1 - 1.0 Pa.s	0.1 - 1.0 Pa.s
Temperature Range	-40 to +150 °C	+10 to +90 °C (ionic, DC) -25 °C to +125 °C (non-ionic, AC)
Stability	Unaffected by impurities	Cannot tolerate impurities
Response Time	< milliseconds	< milliseconds
Density	3-4 g/cm^3	1-2 g/cm^3
$\boldsymbol{\mu_p/\tau^2_{y(field)}}$	10^{-10} to 10^{-11} s/Pa	10^{-7} to 10^{-8} s/Pa
Maximum Energy Density	0.1 Joule/cm^3	0.001 Joule/cm^3
Power Supply	2.25V @ 1-2 A (2-50 watts)	2-5 kV @ 1-10 mA (2-50 watts)

A paper by Nader (2002) outlines that both ER and MR fluids are known for their ability to change their properties in response to external fields, however, recent studies suggest MR

fluids have several advantages over ER fluids. The paper compares and analyses the performance of various semi-active vibration control systems, including MR and ER fluid based systems. Through experimental testing under various vibration conditions, the study found MR fluids to exhibit better performance and energy efficiency. Table 2.1 demonstrates that MR fluids offer significant advantages, including a higher yield stress, greater energy dissipation, and wider range of operating temperatures. Ziabska et. al. (2017) goes further into detail about the negativities of ER fluids regarding its high sensitivity to temperature and humidity changes. This can cause properties to fluctuate unpredictably and make the fluid behave abnormally. In retrospect MR fluids are less sensitive to environmental factors, making them more reliable and consistent in performance. ER fluids are also typically suspended in particles that are highly abrasive, which can cause wear on machinery and components.

2.5 MR Fluid Applications

MR fluids have attracted a lot of interest in recent years due to their unique properties and vast potential applications. Ginder (2013) outlines areas where research has been conducted and applied within the automotive industry such as damping and vibration control, semi active shock absorbers and electrically engaged clutches. The use of MR fluids in the automotive industry allows for electromechanical devices to be created with minimal moving parts, under different applied magnetic fields.

An early article by Carlson, Catanzarite & Clair (1996) discusses the commercial applications for MR fluid devices and provides an overview of the working principles of their applications in various industries, such as automotive, aerospace, and medical. The numerical results presented in the article show that MR fluid devices have significant advantages over traditional mechanical systems. For example, in a shock absorber application an MR fluid device can increase the damping factor force by up to 130%. In the development of a prototype MR fluid damper, which followed a piston-cylinder design, a magnetic field was applied to two plates containing the MR fluid. This configuration resulted in the generation of a damping force measuring 10kN. More recent studies highlighted by Yu et. al. (2022) show that MR rotary dampers can provide controllable and accurate damping, with an increase in stiffness with an increase in current. Research shows that MR dampers are advantageous in response time and low energy consumption and can be divided into rotary and linear dampers. Nguyen

& Choi (2009) optimised a linear flow mode MR shock absorber for vehicle suspension. The MR shock absorber can reduce the vibration of the vehicle by 70% and increase energy dissipation by up to 110% compared to conventional hydraulic options. Giorgetti et. al. (2010) designed a rotational MR damper for the front-wheel suspension of a compact car. Through experimental analysis, their findings demonstrated that the MRF damper exhibited efficient damping characteristics across a broad spectrum of frequencies and amplitudes, while also having a swift response time.

Jamadar et. al. (2023) presents an MR fluid damper using Lord Corporation's 132-DG (Figure 2.4). The piston core is wound with 240 turns of 26AWG copper wire to make the electromagnetic coil. The purpose of the study was to develop a more affordable MR damper, with better performance over current passive dampers. The results showed that the MR damper improved the ride comfort by 17.6% at 20 km/hr and the handling by 29.3%. The study also investigated the thermal effects on the MR fluid with no leakage or performance issues noted when enduring excitation cycles at temperatures as high as 120°C.

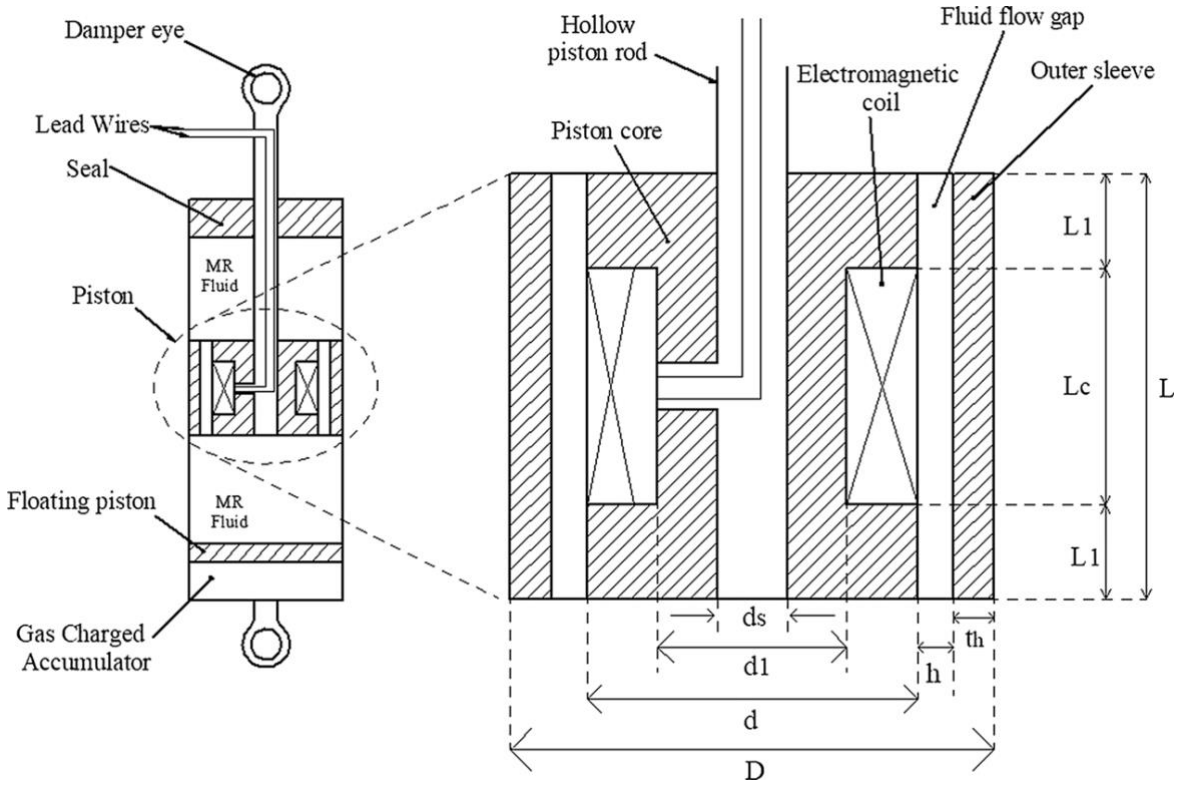

Figure 2.4 MR fluid damper schematic (Jamadar et. al. 2023)

The current research and technology surrounding MR fluids shows that further research is required before it can be commercialised within certain applications such as braking mechanisms. The following section provides a literature review on MR fluid brake designs to gather an understanding of challenges faced in previous research, and how this can be overcome to develop an effective design solution.

2.6 MR Fluid Brake Designs

Park et. al. (2006) proposes a braking system that can be constructed using rotating disks submerged in MR fluid and enclosed in an electromagnet. The yield stress of the fluid is modified in response to the magnetic field, thereby generating friction on the surface of the rotating disks and producing braking torque. The paper suggested the incorporation of a conventional hydraulic brake as a backup in the event of an ECU failure, while consolidating all brake control functions into a single main electronic control unit. Electronically controlled brake systems can be advantageous over hydraulic braking systems due to their easy adaption and behaviour changes by altering the software parameters and electrical outputs. In addition, this enables the effortless integration of both existing and novel control functionalities, such as ABS and vehicle stability control. The present study suggests the implementation of an MR actuator in each wheel's brake system, which allows modulation of the brake torque through adjustments to the DC current flowing through the electromagnet. MR fluids exhibit a linear response, wherein the increase in stiffness is directly proportional to the applied magnetic field strength as outlined in a previous paper by Yu et. al. (2022). Park et. al. (2006) outlines that the proposed MRB brake can be further improved by inserting slots/holes in the rotating disk to mitigate structural weight and improve heat dissipation. Figure 2.5 shows the temperature distribution to be significantly higher within the rotating disk and the surround MR fluid.

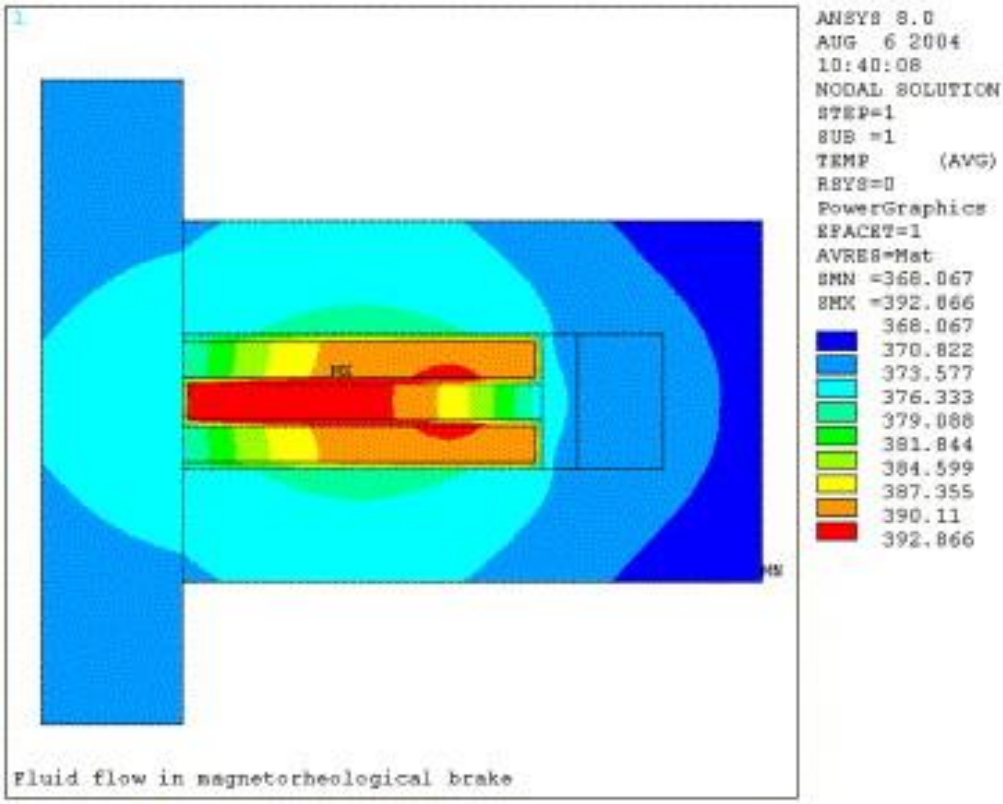

Figure 2.5 Temperature distribution within MRB (Park et. al. 2006)

Both Falcão da Luz (2002) and Park et. al. (2006) explain that conventional hydraulic braking systems have a 200-300ms delay between the time the brake pedal is applied to the corresponding brake response. An MR fluid brake can drastically reduce this to 15-25ms further reducing braking distance. The proposed design for the MR brake actuator can be seen in Figure 2.6, showing a disk rotating within MR fluid enclosed in a static casing.

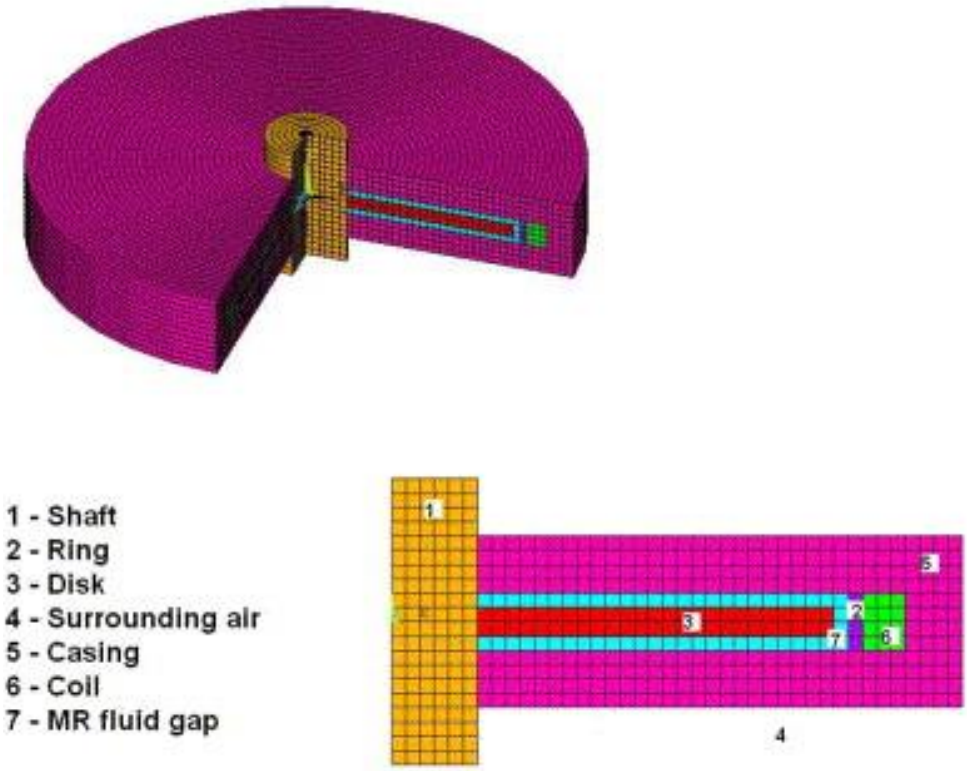

Figure 2.6 Experimental setup of MR brake designs (Park et. al. 2006).

Karakoc, Park & Suleman (2008) presents an MR brake design like the one in the previously mentioned paper by Park et. al. (2006). However, more thought has been put into selecting a material that has the perfect magnetic, structural, and thermal properties. Ferromagnetic substances have a non-linear permeability that alters with both temperature and the strength of the magnetic field. After weighing factors such as cost, availability, and permeability, AISI 1018 low carbon steel was selected as the magnetic material for the magnetic circuit, including both the core and the disks. For structural purposes, the shaft was made of 304 stainless steel due to its high yield stress. Karakoc, Park & Suleman (2008) highlights the importance of removing the heat from the brake as quickly as possible, therefore a material with high conductivity, such as aluminium, was used for the non-magnetic brake components. It is crucial to remove heat from the braking system because of the temperature-dependent permeability of ferromagnetic materials and the viscosity of the MR fluid. An overview of the experimental setup is presented below in Figure 2.7.

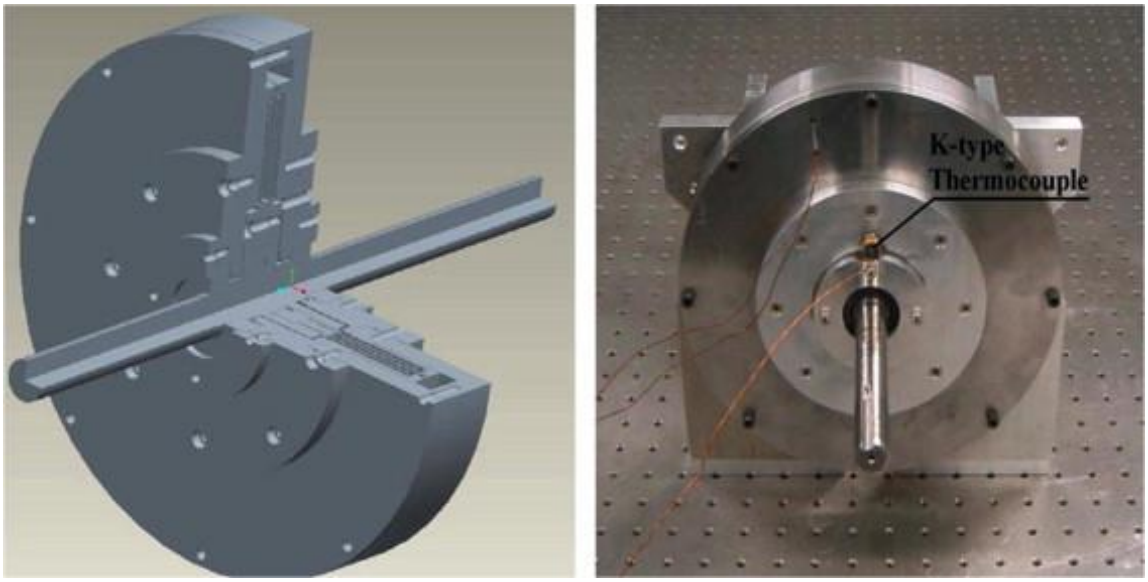

Figure 2.7 Experimental setup of MR Fluid Brake (Karakoc, Park & Suleman 2008)

The literature showed a linear relationship between braking torque and the rotational speed as shown in Figure 2.8. After the viscous torque was calculated, the current was applied to the electromagnet coil and subsequent torque measurements were taken.

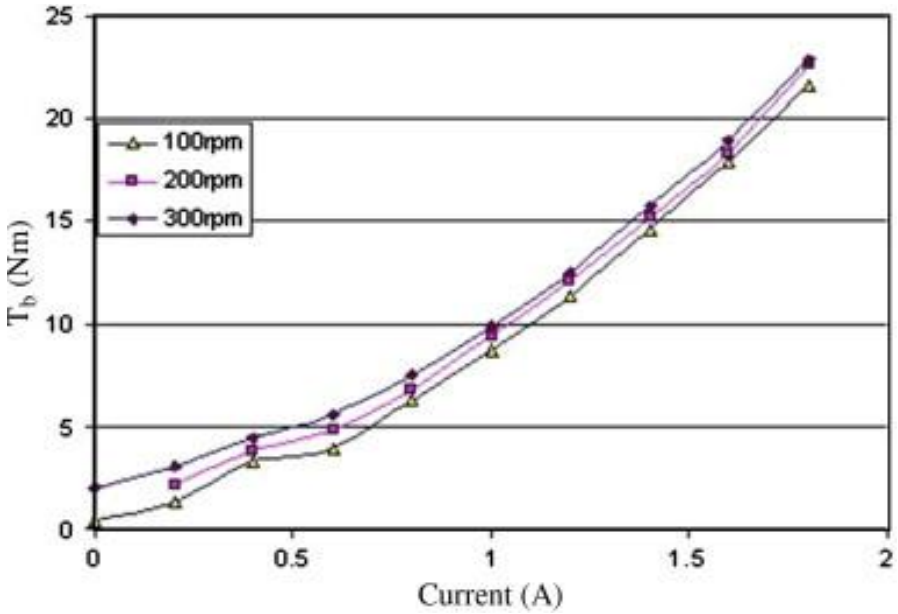

Figure 2.8 Linear Relationship between braking torque and rotational speed (Karakoc, Park & Suleman 2008)

The paper also highlights the criticality of sealing the MR fluid due to the contaminant iron particles. In the design this is proposed with dynamic o-rings, static o-rings and sealant as shown in Figure 2.9. According to the article, the generated torque was affected by temperature

variations, as they impact the viscosity and magnetic properties of the MR fluid, resulting in significant heat buildup. The findings indicate that each brake was only capable of producing 5% of the required 500Nm braking torque for passenger vehicles. To meet the requirements, the paper suggests adding more disks or relaxing the size and weight constraints. In previous research, a simulation of a 27.8kg MR brake design with relaxed size and weight restrictions generated 100Nm of braking torque.

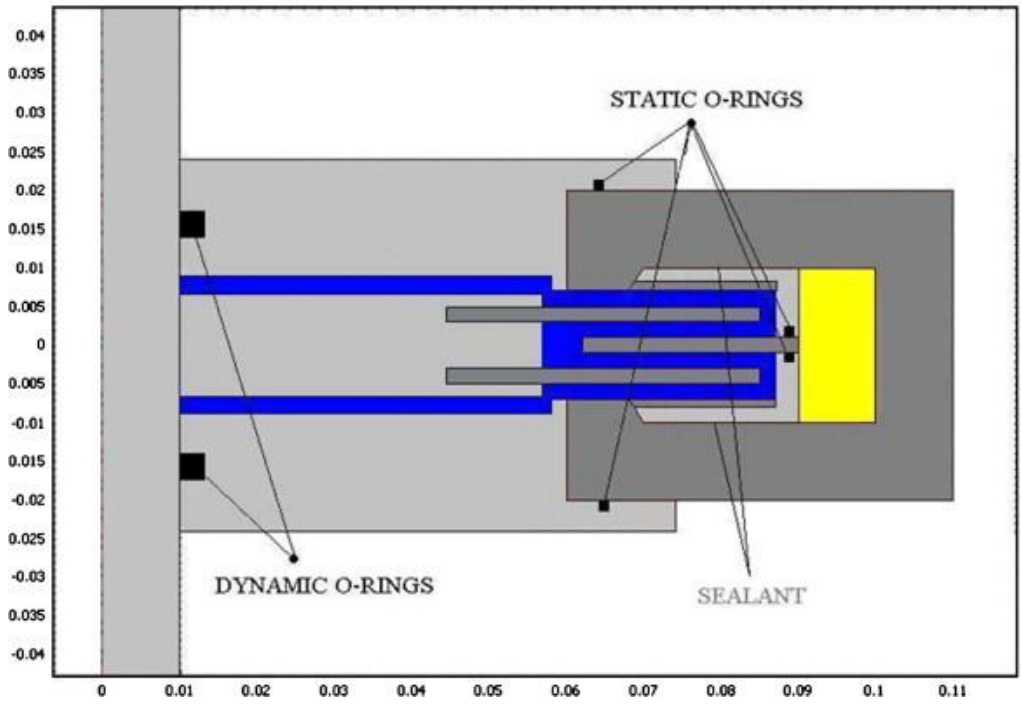

Figure 2.9 MRB design schematic to seal fluid in casing (Karakoc, Park & Suleman 2008)

Li & Du (2003) introduced an MRB design that features two stationary casings and a rotating disk enclosed within, with MR fluid filling the gap between the two components. To achieve optimum results, the fluid gap between the disk and casings must be considered. A smaller constant gap is proposed to provide a uniform distribution of the magnetic flux, with practical gaps ranging from 0.25mm to 2mm. This is confirmed in a paper by Yoo & Wereley (2002) where a design was explored for a meso-scale MR valve, with the performance being evaluated across different fluid gap parameters. The results show that the maximum magnetic flux density was achieved in gaps ranging from 0.5mm to 2mm. Li & Du (2003) also incorporates mixing pins to ensure the fluid stays in a slurry state and the system remains dynamically balanced. Figure 2.10 shows the schematic design of the MRB with the mixing pins (5) attached to the rotor (9), enclosed within the left and right housings (4 & 5).

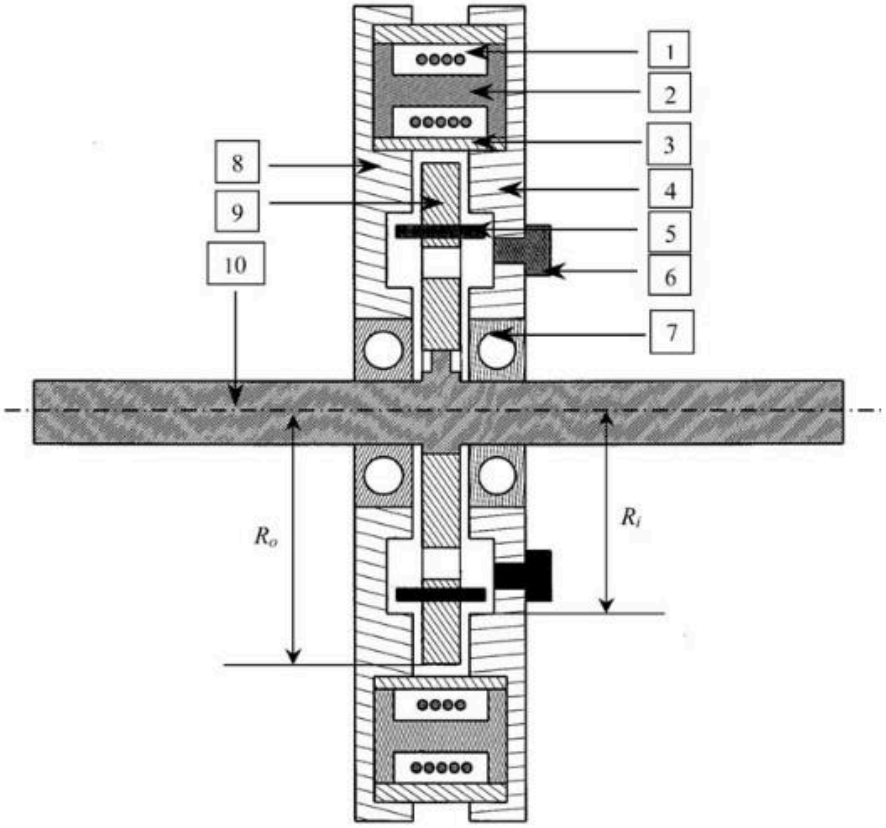

Figure 2.10 MRB schematic with mixing pins to prevent slurry state of fluid (Li & Du 2003)

References

- Acerbi, E & Mingione, G, 2002, 'Regularity Results for Stationary Electro-Rheological Fluids', doi:10.1007/s00205-002-0208-7

- Ahamed, R, Choi, S.B., Ferdaus, M.M., 2018, 'A state of the art on magneto-rheological materials and their potential applications', *Journal of Intelligent Material Systems and Structures,* vol. 29, no. 10, pp. 2051-2095, doi:10.1177/1045389X18754350

- Carlson, J.D., Catanzarite, D.M. & Clair, St., 1996, 'Commercial Magneto-rheological Fluid Devices', *International Journal of Modern Physics B*, vol. 10, no. 23, doi:10.1142/S0217979296001306

- Dakhil, M.H., Rai, A.K., Reedy, R. and Jabbar, A.A., 2014, 'Structural Design and Analysis of Disk Brakes in Automobiles', *International Journal of Mechanical and Production Engineering Research and Development,* vol. 4, pp.95-112.

- Falcão da Luz, L 2002, 'Design of a Magnetorheological Brake System', Masters of Applied Science, Instituto Superior Técnico, Lisboa.

- Ginder, JM 2013, 'Behaviour of Magnetorheological Fluids', *Journal of Engineered Proteins as Multifunctional Materials,* vol. 23, no. 8, pp. 26-29, doi:10.1557/S0883769400030785

- Giorgetti, A, Baldanzini, N, Biasiotto, M & Citti, P, 2010, 'Design and testing of a MRF rotational damper for vehicle applications', *Journal of Smart Materials and Structures,* vol. 19, no. 6, doi:10.1088/0964-1726/19/6/065006

- Gopinath, B & Sathishkumar, G.K 2021, 'A systematic study of the impact of additives on structural and mechanical properties of Magnetorheological fluids', *Materials Today: Proceedings*, vol. 37, pp. 1721-1728, doi:10.1016/j.matpr.2020.07.246

- Hao, T, 2001, 'Electrorheological Fluids', *Journal of Advanced Materials,* vol. 13, no. 24, pp. 1847-1857, doi:10.1002/1521-4095(200112)13:24

- Jamadar, M.H., Devikiran, P, Desai, R.M., Kumar, H & Joladarashi, S, 2023, 'Real-time testing and thermal characterisation of a cost-effective magneto-rheological (MR) damper for four-wheeler application', *Journal of the Brazilian Society of Mechanical Sciences and Engineering,* vol. 45, no. 95, doi: 10.1007/s40430-023-04035-x

- Joe, Y.G., Cha, B.G., Sim, H.J., Lee, H.J. & Oh, O.H., 2007, 'Analysis of Disc Brake Instability Due to Friction-Induced Vibration Using a Distributed Parameter Model', *International Journal of Automotive Technology,* vol. 9, no. 2, pp. 161-171, doi:10.1007/s12239-008-0021-x.

- Jolly, M, Carlson, J & Muñoz, B 1996, 'A model of the behaviour of magnetorheological materials', *Journal of Smart Material and Structures,* vol. 5, no. 5, pp. 607, doi:10.1088/0964-1726/5/5/009

- Karakoc, K, Park, E.J & Suleman, A 2008, 'Design Considerations for an Automotive Magnetorheological Brake', *Journal of Mechatronics,* vol. 18, no. 08, pp. 434-447, doi:10.1016/j.mechatronics.2008.02.003

- Kumar, J.S., Paul, P.S., Raghunathan, G & Alex, D.G 2019, 'A review of challenges and solutions in the preparation and use of magnetorheological fluids', *International Journal of Mechanical and Materials Engineering,* vol. 14, no. 13, doi:10.1186/s40712-019-0109-2

- Leen, G, Heffernan, D, 2002, 'Expanding Automotive Electronic Systems' *Journal of Computer*, vol. 35, no. 1, pp. 88-93, doi:10.1109/2.976923

- Li, W.H. & Du, H., 2003, 'Design and Experimental Evaluation of a Magnetorheological Brake', *The International Journal of Advanced Manufacturing Technology*, vol. 21, pp. 508-515, doi: 10.1007/s001700300060

- Nader, J, 2002, 'A Comparative Study and Analysis of Semi-Active Vibration-Control Systems', *Journal of Vibration and Acoustics*, vol. 140, no. 4, pp. 593-605, doi:10.1115/1/1500336

- Nguyen, Q.H., Choi, S.B., 2012, 'An analytical approach to optimally design of electrorheological fluid damper for vehicle suspension system', *Meccanica,* vol. 47, pp. 1633-1647, doi: 10.1007/s11012-012-9544-3

- Nguyen, Q.H. & Choi, S.B., 2009, 'Optimal design of MR shock absorber and application to vehicle suspension', *Journal of Smart Materials and Structures,* vol. 18, no. 3, doi:10.1088/0964-1726/18/3/035012

- Park. E. J, Stoikov, D, Falcao Da Luz, L & Suleman, A 2006, 'A performance evaluation of an automotive magnetorheological brake design with a sliding mode controller', *Journal of Mechatronic*, vol. 16, no. 07, pp 405-416, doi:10.1016/j.mechatronics.2006.03.004

- Park. E. J, Stoikov, D, Falcao Da Luz, L & Suleman, A 2006, 'A performance evaluation of an automotive magnetorheological brake design with a sliding mode controller', *Journal of Mechatronic*, vol. 16, no. 07, pp 405-416, doi:10.1016/j.mechatronics.2006.03.004

- Raju, K.R. & Varma D.V., 2017, 'Developments in vibration control of structures and structural components with magneterheological fluids', *Journal of Current Science*, vol. 112, no. 3, pp. 499-508

- Sau, A.K., Pulinat, K.G., Moss, P.N., Ranjeet, P & Prabu, S.S, 2022, 'A comparative study on the thermal and dynamic analysis of a disc brake using Ansys', *International Conference on Materials and Sustainable Manufacturing Technology*, vol. 65, no. 08, doi:10.1016/j.matpr.2022.06.318

- Seung-Bok, C, Young-Min, H & Kum-Gil, S, 2008, 'Vibration Control of Vehicle Suspension System Featuring ER Shock Absorber', *International Journal of Applied Electromagnetics and Mechanics,* vol. 27, no. 3, pp. 189-204, doi:10.3233/JAE-2008-927

- Stanway, R, 2004, 'Smart fluids: Current and Future Developments', *Materials Science and Technology,* vol. 20, no. 8, pp. 931-939, doi:10.1179/026708304225019867

- Stanway, R, Sproston, J.L. and El-Wahed, A.K., 1996, 'Applications of electro-rheological fluids in vibration control: a survey', *Journal of Smart Materials and Structures,* vol. 5, no. 4, doi:10.1088/0964-1726/5/4/011

- Sturk, M, Wu, X.M., Wong, J.Y., 2007, 'Development and Evaluation of a High Voltage Supply Unit for Electrorheological Fluid Dampers', *International Journal of Vehicle Mechanics and Mobility,* vol. 24, no. 2, pp. 101-121, doi:10.1080/00423119508969083

- Thakur, A.S., 2018, 'Thermal Analysis of Disc Brake Using ANSYS', *International Journal of Technical Innovation in Modern Engineering & Science,* vol. 04, no. 06, doi: 10.13140/RG.2.2.20351.97441

- Yoo, J.H. & Wereley, N.M., 2002. 'Design of a high-efficiency magnetorheological valve', *Journal of Intelligent Material Systems and Structures*, vol. 13, no. 10, pp. 679-685.

- Yu, J, Dong, X, Su, X & Qi, S., 2022, 'Development and characterisation of a novel rotary magnetorheological fluid damper with variable damping and stiffness', *Journal of Mechanical Systems and Signal Processing,* vol. 165, doi: 10.1016/j.ymssp.2021.108320

- Ziabska, E, Duchowski, J, Olszak, A, Osowski, K, Kesy, A, Kesy, Z & Choi, S.B., 2017, 'Wear forms of heterogeneous electro-rheological fluids working in a hydraulic clutch system', *Journal of Smart Materials and Structures,* vol. 26, no. 9, doi:10.1088/1361-665X/aa78dc

Analysis of Vickers Microhardness Test to Determine Case Depth of Low & Medium Carbon Steels

MEC301: Lab Report

Lachlan Wensley

St No: 1109326

Abstract

Surface hardening is used to change a components surface carbon content while resulting in a ductile core, further improving the wear resistance. Many engineering applications optimise this process especially with components that have large loads and contact. This report aims to analyse the microhardness and calculate the case depth for two carbon steel samples. A DuraScan microhardness machine with a diamond pyramid indenter was used to measure the Vickers hardness values for a 0.15% low carbon steel, and a 0.35% medium carbon steel sample. 24 tests were done at 0.1mm increments with 100gf. The heat treated 0.15% low carbon steel sample recorded a case depth of 0.23mm, and the case hardened 0.35% medium carbon steel sample had a case depth of 1.49mm. These results matched the theories and literature regarding microhardness in case hardened steels. Heat treatments were developed to optimise the microstructure of the components and a diffusion time of 278 seconds and 9106 seconds was calculated for the 0.15% low carbon steel, and the 0.35% medium carbon steel respectively.

1. Introduction

Heat treatment processes are generally implemented in the engineering field to produce optimum carbon steel components. Surface hardening is used to change a components surface carbon content while resulting in a ductile core. This improves the wear resistance and resistance to plastic deformation. (D. Callister Jr & G. Rethwisch). There are various methods of surface hardening processes such as carburizing, carbo-nitriding and induction hardening. For materials with a carbon content of 0.3% or less carburizing must be used. The purpose of carburizing is to increase the content of carbon on the surface to improve the case hardness of the component. This is done by diffusing carbon into the surface layer in a high temperature environment followed by quenching. The distance that the carbon content diffuses into the components surface is known as the case depth (Venkatesh & Rajesh 2014). This is commonly done on automotive parts with large amounts of contact and loading. It is important in engineering applications to test the surface hardness of materials to make sure they meet the reliability required. Common forms of microhardness tests are the Rockwell, Brinell and Vickers hardness tests which are effective ways of measuring surface hardness due to their non-destructive method. The Vickers hardness test uses a diamond pyramid indenter and is suitable for materials with high hardness, or samples that might not be macroscopically flat (R. Askeland et al. 2010). In theory case hardened steels will have a higher Vickers Hardness than heat treated samples with a lower carbon content.

2. Experimental

A Vickers microhardness test was done on two cross sectional steel samples mounted in Bakelite. Sample 1 was from a heat-treated case ring with a carbon content of 0.15%, while sample 2 was from a case-hardened steel block with a carbon content of 0.35%. A Struers DuraScan machine using a diamond pyramid indenter was used to apply 24 indentations at 0.1mm increments with a 100gf penetration force for each sample. The Struers DuraScan machine used a diagonal indentation measurement to calculate the Vickers Hardness score which was recorded in Table A1. A representation of the indentation angle (136^{o}) and measurement can be seen in Figure 1.

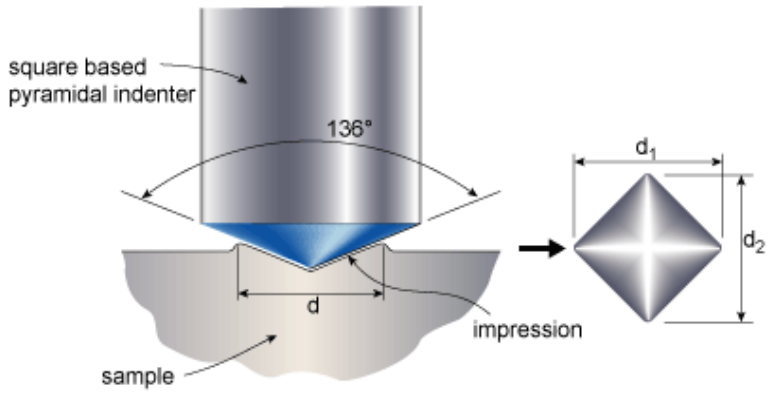

Figure 1: Indentation angle and measurement representation for Vickers Hardness test (Alhashmy 2012).

3. Results and Discussion

3.1 Analysis of Case Depth and Photographic Evidence

From graphical analysis and interpolation, the case depth was calculated for both materials. The case depth for the heat-treated case ring made from 0.15% low carbon steel was 0.23mm and 1.49mm for the case hardened 0.35% medium carbon steel block. The case depths of steels are strongly influenced by the carbon potential control when carburizing. Factors such as the gas composition, pressure, and operating temperature all strongly effect these outcomes (Venkatesh & Rajesh 2014). It can be seen from Figure 2 that the process of case hardening provides a significantly higher Vickers Hardness value for components. The 0.15% low carbon steel has a sudden drop in hardness approximately 0.25mm from the edge, whereas the 0.35% medium carbon steel has a gradual decrease in hardness throughout (Figure 2).

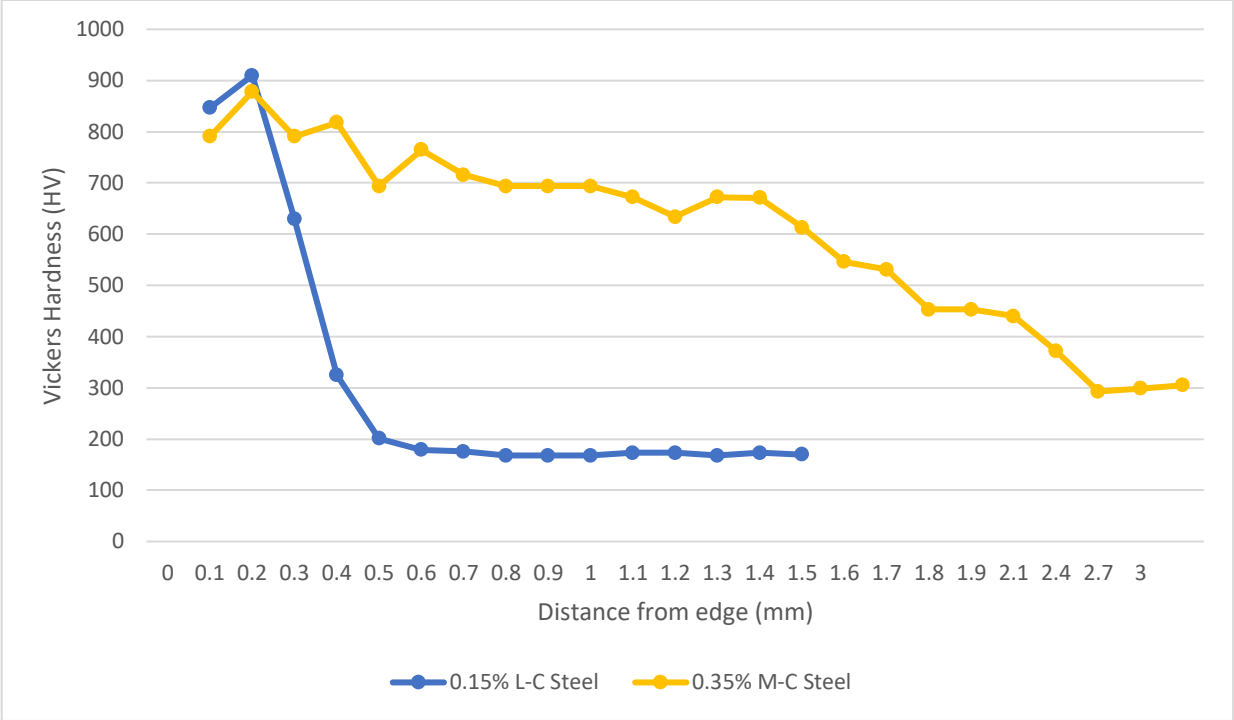

Figure 2: Vickers Hardness scores measured for 0.15% low carbon steel and 0.35% medium carbon steel

The initial indentation at test point two (Figure 3) for 0.15% low carbon steel and 0.35% medium carbon steel showed a similar Vickers hardness of 910 and 878 respectively. The following indentations for the 0.15%C sample show a significant reduction in Vickers hardness dropping to 630 and 325 just 0.3mm into the surface. When the 0.15%C sample reaches test point six (Figure 4) it begins to plateau at a Vickers hardness of approximately 170. The 0.35%C steel undergoes a gradual decrease in Vickers hardness and at its final test point (Figure 4) 2.3mm from the edge, a Vickers hardness of 305 was measured. From Figure 4, at test point 23 the 0.35%C has a similar indentation size to test point seven of the 0.15%C sample. After 23 test points the Vickers hardness of the 0.35%C steel was 1.7 times greater than that of the 0.15%C sample.

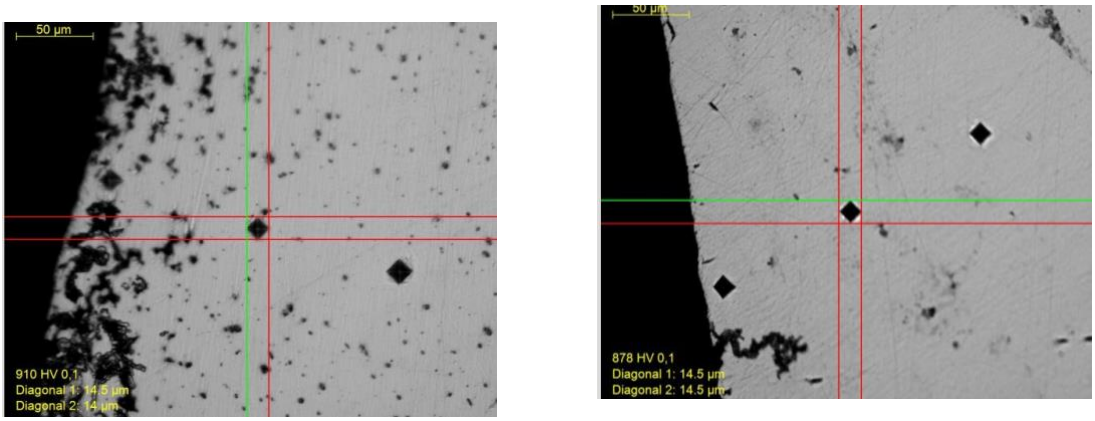

Figure 3: Initial indentation (T2) of 0.15% low carbon steel (left) and 0.35% medium carbon steel (right)

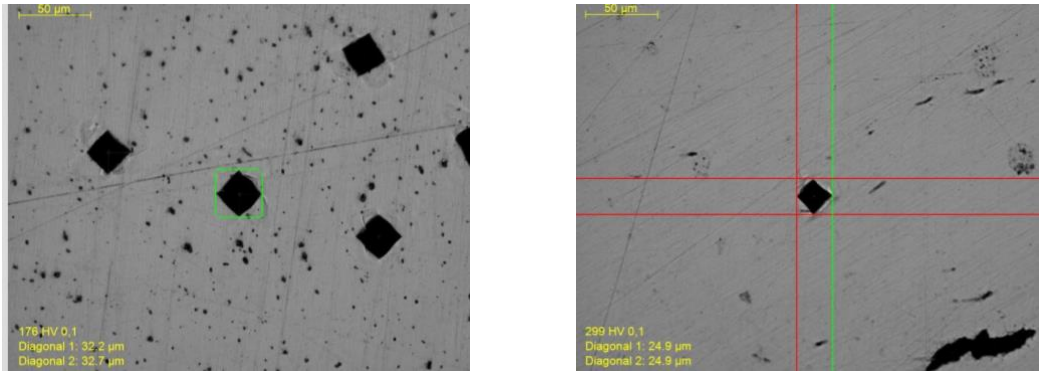

Figure 4: Final indentation (T7, T23) of 0.15% low carbon steel (left) & 0.35% carbon steel (right)

3.2 Heat treatment plan for 0.15% & 0.35% carbon components and Diffusion Theory

Using values from Callister, a suitable heat treatment plan can be developed for the 0.15% low carbon steel component and the 0.35% medium carbon steel component. From Fick's second law (Equation 1) the diffusive time needed for the components to develop a case depth of 0.23mm and 1.49mm respectively can be calculated.

For both the components the material must be pack carburized (diffused) at an austenite temperature of 1100^{o} Celsius. This involves placing the components in a high carbon medium such as carbon powder and heating in a furnace. At the high temperature the reduction reaction occurs, and the surrounding carbon is diffused into the component (Negara & Wildiyarta 2019).

Using Equation 1 a required diffusive time of 278 seconds and 9106 seconds was calculated for the 0.15% low carbon steel, and the 0.35% medium carbon steel respectively. After the component completes the case hardening process (carburisation), it is then quenched to form a martensite structure. When quenched suddenly from the austenite phase a martensite structure is formed as the steel is not given enough time for diffusion. This develops a supersaturated state and restricts the motion of dislocations increasing the hardness in the steel (F. Smith et al. 2019).
While having an increase in hardness this does affect the components brittleness, but this can be avoided by tempering and cooling at a specific rate to optimise hardness. From these heat treatment plans, carburising for longer periods results in a greater case depth further increasing the hardness of the component.

$$\frac{C_x - C_o}{C_s - C_o} = 1 - erf\left(\frac{x}{2\sqrt{Dt}}\right) \quad (1)$$

4. Conclusions

- After analysis and calculations, the experiment on 0.15%C and 0.35%C samples does verify the theory of case-hardened materials.
- It was recorded that the 0.35% medium carbon steel component recorded a larger case depth and hardness then the 0.15% low carbon steel.
- Heat treatment plans can be used to improve the hardness of steels and optimise components. To establish a case hardening on the samples, a carburisation time of 278 seconds was calculated for the 0.15% low carbon steel, and 9106 seconds for the 0.35% medium carbon steel.

- The microhardness experiment had minimal error due to all calculations being done by the DuraScan machine, hence all hardness values were considered accurate.

References

- Alhashmy, H 2012, “Fabrication of Aluminium Matrix Composites (AMC’s) by Squeeze Casting Techniques Using Carbon Fibre as Reinforcement”, vol. 1, no. 1,.
- D. Callister Jr, W & G. Rethwisch, D 2018, *Materials Science and Engineering*, 10th edn, Wiley.
- F. Smith, W. Hashemi, J & Presuel-Moreno, D 2019, *Foundations of Materials Science and Engineering*, 6th edn, McGraw-Hill Education, New York.
- Negara, D & Widiyarta, M 2019, “The study on mechanical properties of pack carburized low carbon steel using BaCO as energizer”, *IOP Conference Series: Materials Science and Engineering,* vol. 673, no. 1.
- R. Askeland, D, P. Fulay, P & J. Wright, W 2010, *The Science and Engineering of Materials*, 6th edn, Wiley
- Venkatesh, J & Rajesh, A 2014, “Evaluation and Diffusion Assessment for Surface Hardening Processes”, *Journal of Material Science & Engineering*, vol. 03, no 03.

Appendix

Table A1: Results of Vickers Hardness (HV) test and x distance from edge (mm).

	0.15% Low Carbon Steel		**0.3% Medium Carbon Steel**	
Test Location	Vickers Hardness (HV)	X distance from edge (mm)	Vickers Hardness (HV)	X distance from edge (mm)
1	847	0	791	0
2	910	0.1	878	0.1
3	630	0.2	791	0.2
4	325	0.3	818	0.3
5	201	0.4	694	0.4
6	179	0.5	765	0.5
7	176	0.6	716	0.6
8	168	0.7	694	0.7
9	168	0.8	694	0.8
10	168	0.9	694	0.9
11	173	1.0	672	1.0
12	173	1.1	634	1.1
13	168	1.2	672	1.2
14	173	1.3	671	1.3
15	170	1.4	613	1.4
16			546	1.5
17			531	1.6
18			453	1.7
19			453	1.8
20			440	1.9
21			372	2.0
22			293	2.1
23			299	2.2
24			305	2.3

The Effects of Varying Flow Rate on Parallel and Counter Flow Heat Exchanger Arrangements

By Lachlan Wensley, ID# 1109326

1.0 Introduction

1.1 Theory of Heat Exchangers

Heat exchangers are used to transfer heat between fluids at different temperatures without directly mixing with each other. The heat transfer process involves convection from the hot fluid to the wall, conduction through the wall, and convection from the wall to the cold fluid. The concentric tube heat exchanger consists of a fluid flowing through a smaller diameter pipe overlapped by fluid flowing in a larger diameter pipe (Çengel & Ghajar 2015). Plate heat exchangers consist of several plates with corrugated flat flow passages which enables colder fluid to be surrounded by two hot fluid streams. Pipe orientation can either be parallel (fluids entering from the same position) or in a counter flow arrangement (fluids entering from the opposite position). Heat exchangers are considered as steady flow devices, deeming the mass flow rate constant, and leaving the fluid properties and velocities the same, which defines the kinetic and potential energies as negligible (Huang 1989).

Understanding the process and application of heat exchangers is crucial in engineering whether it be to choose a heat exchanger that will accomplish a required temperature change, or to predict the outlet temperatures of fluid streams. Previous theory states that, counter flow arrangement will be more efficient than parallel flow arrangement due to the constant temperature difference (Schlunder 1983). This experiment will be used to verify these findings for different flow rates in concentric tube and parallel flow heat exchangers.

1.2 Governing Equations

The log mean temperature difference (LMTD) shows the average temperature difference between the hot and cold fluids (Equation 1). The LMTD can be used to achieve a specific temperature change in a fluid stream if a mass flow rate is known (Forsberg 2021). Equation 2

shows the heat transfer coefficient which is a measurement of how well the exchanger operates. Equation 3 shows the energy balance coefficient which displays the relationship between the energy emitted and the energy absorbed.

$$LMTD = \frac{(T_{H2} - T_{C2}) - (T_{H1} - T_{C1})}{ln(\frac{T_{H2} - T_{C2}}{T_{H1} - T_{C1}})} \quad (1)$$

$$U = \frac{\dot{Q}_e}{A * LMTD} \quad (2)$$

$$C_{EB} = \frac{\dot{Q}_a}{\dot{Q}_e} \quad (3)$$

2.0 Methodology

Using parallel configuration, a TD360a concentric tube heat exchanger (Figure 1b) was used with a 60℃ hot flow rate of 3.0L/min with a variable cold flow rate of 3.0, 2.0, 1.0 and 0.5L/min. The inlet, average and outlet temperatures were recorded after 5 minutes of operation. The previous method was repeated with a counter flow arrangement with the cold water intake reversed. After all flow rates underwent testing a TD360b plate heat exchanger (Figure 1c) was installed and the parallel and counter flow methods were repeated with three minute intervals. From the recorded data, factors such as density and specific heat were calculated and recorded in Appendix 1.

Figure 1a: Parallel and Counter flow in a concentric tube heat

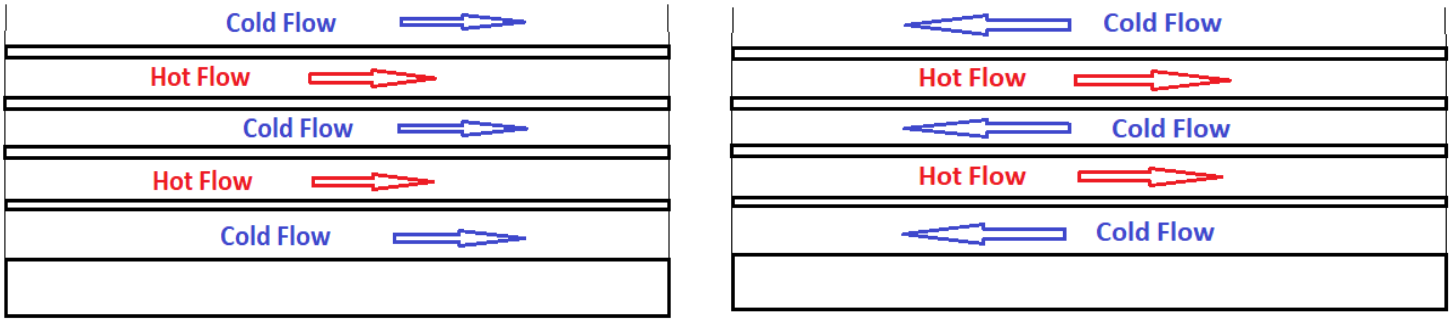

Figure 1b: Parallel and Counter flow arrangements in a plate heat exchanger

3.0 Results & Discussion

Figures 3-6 show the effects parallel and counterflow arrangements have on concentric tube and plate heat exchangers. The hot flow rate was set as 3.0L/min for all tests with a varying cold flow rate. The inlet and outlet temperatures were recorded, and the average temperature of each flow was calculated to assist with governing equations. This enabled the calculation of the log mean temperature difference, the heat transfer coefficient, and the energy balance coefficient.

Figure 3 shows the effects of parallel flow within the concentric tube heat exchanger with a cold flow rate of 3.0L/min (test 1) and 0.5L/min (test 4). Test 1 shows a similar temperature gradient for both hot and cold flows with a change in temperature of ≈ 5.20℃. This coincided with a log mean temperature difference (Equation 1) of 29.90℃ and a heat transfer coefficient

(Equation 2) of 1756.33 W/m^2/K. Test 4 shows a steep temperature gradient for cold flow with a temperature difference of 13.3℃. The hot flow experienced a reduction in gradient with a temperature difference 2.2℃. For test 4 the log mean temperature difference was 26.70℃ with a heat transfer coefficient of 847.83 W/m^2/K.

Figure 4 shows the effects of counter flow on concentric tube heat exchangers with a cold flow rate of 3.0L/min (test 1) and 0.5L/min (test 4). Test 1 displayed a uniform gradient across hot and cold flows with a temperature difference of ≈ 5.00℃. Test 4 displayed a similar situation to parallel flow with a steep cold flow gradient and a reduced gradient for hot flow. The log mean temperature difference for test one was 29.62℃ and 26.75℃ for test four with a heat transfer coefficient of 1703.80 W/m^2/K and 884.71 W/m^2/K respectively.

A negligible difference in data of < 4% was seen across Figure 3 and 4 deeming the effectiveness of parallel and counter flow arrangements the same for concentric tube heat exchangers under both flow rates.

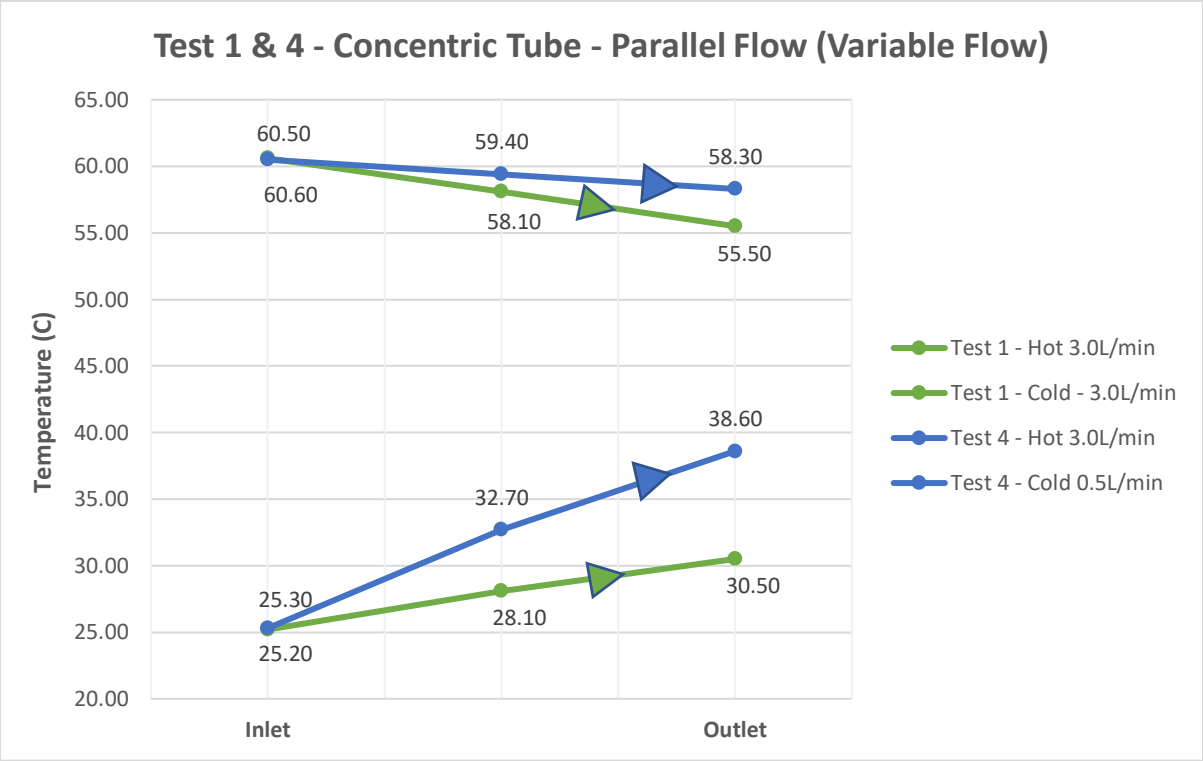

Figure 3: Test 1 shows parallel flow within the concentric tube with a cold flow rate of 3.0L/min. Test 4 displays a cold flow rate of 0.5L/min.

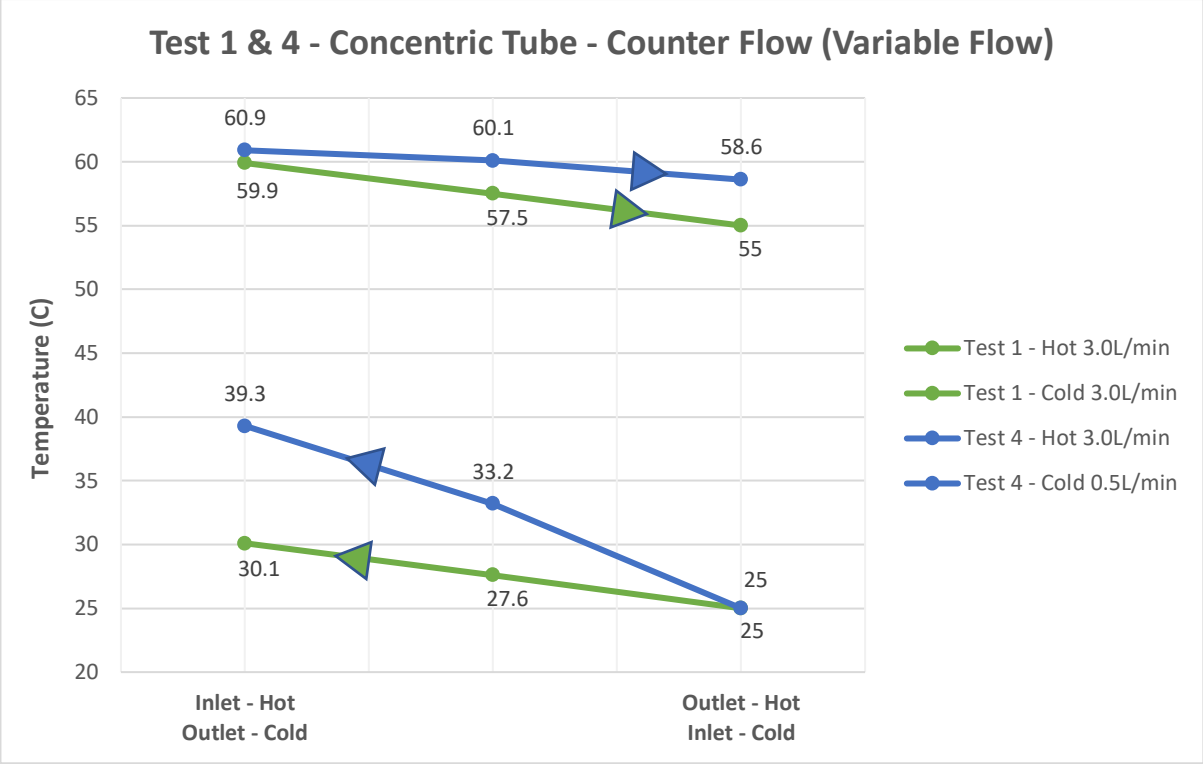

Figure 4: Test 1 shows counter flow within the concentric tube with a cold flow rate of 3.0L/min. Test 4 displays a cold flow rate of 0.5L/min.

Figure 5 presents the effects of parallel flow on a plate heat exchanger with varying cold flow rates of 3.0L/min (test 1) and 0.5L/min (test 4). For test one a temperature difference was calculated of 5.1℃ and 2.6℃ for hot and cold flows respectively. This shows that the cold flow had a reduction in gradient with comparison to the concentric tube heat exchanger. Test 4 displays the same steep cold flow gradient as Figures 3 & 4 with a temperature difference of 13.30℃ and a reduced hot flow gradient. The log mean temperature difference for test one was 31.69℃ and 26.70℃ for test four with a heat transfer coefficient of 1656.88 W/m^2/K and 847.83 W/m^2/K respectively.

Figure 6 displays a counter flow arrangement within the plate heat exchanger. In test 1 a minor temperature difference of 2.5℃ is seen for both hot and cold flows. This correlates with a log mean temperature difference of 32.98℃ and a heat transfer coefficient of 780.06 W/m^2/K.

Test four shows a reduction in temperature gradient compared to previous tests with a temperature difference of 1.5℃ for hot flow and 8.2℃ for cold flow. This aligns with a log mean temperature difference of 31.10℃, with a heat transfer coefficient of 496.18 W/m^2/K.

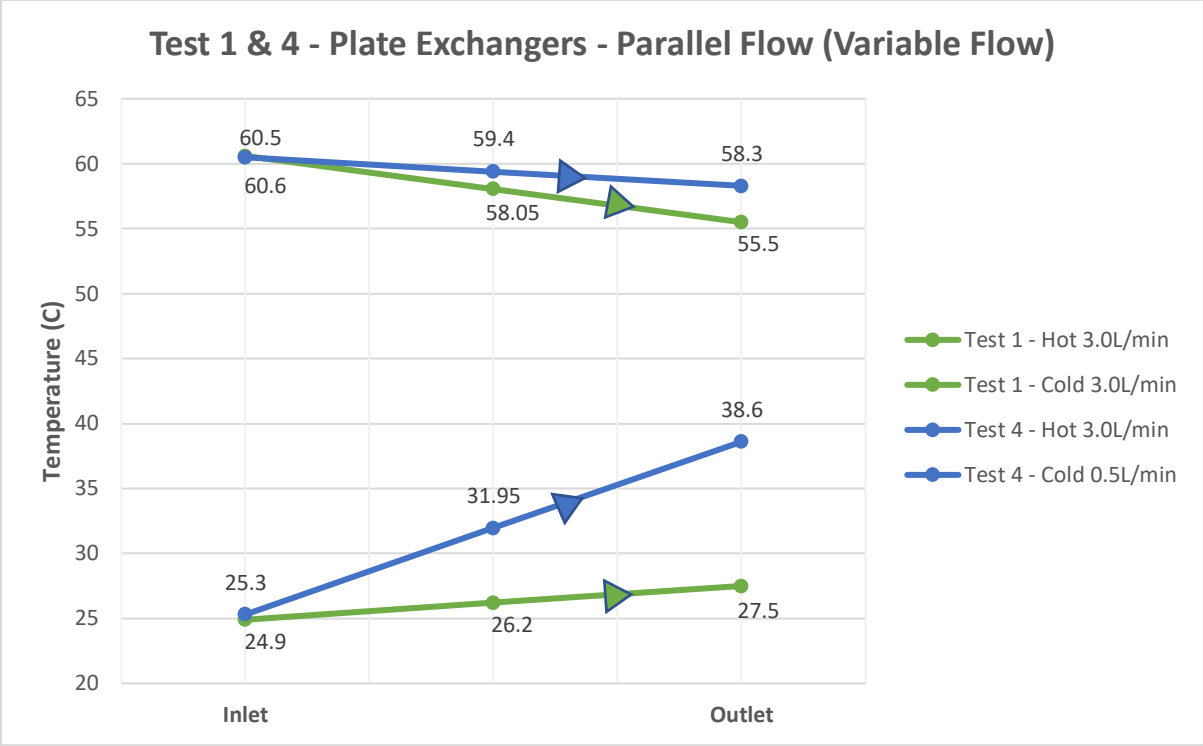

Figure 5: Test 1 shows parallel flow within the plate heat exchanger with a cold flow rate of 3.0L/min. Test 4 shows a cold flow rate of 0.5L/min.

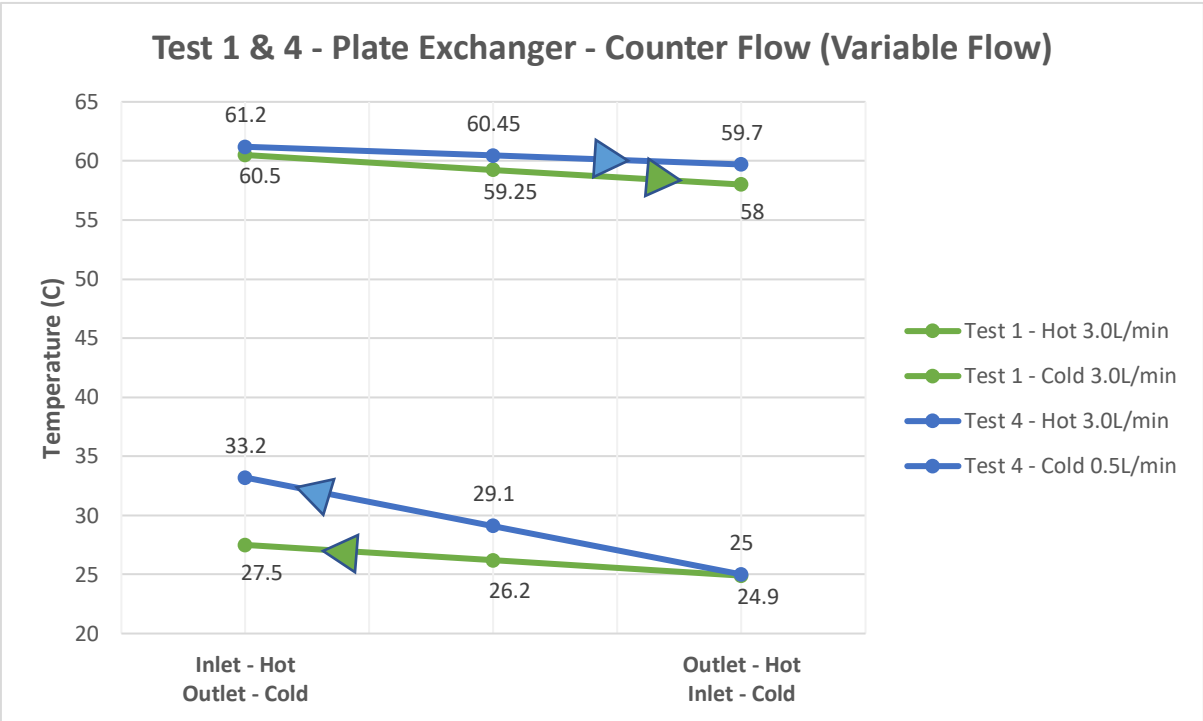

Figure 6: Test 1 shows counter flow within the plate heat exchanger with a cold flow rate of 3.0L/min. Test 4 shows a cold flow rate of 0.5L/min.

Figures 7 & 8 displays cold flow rate and energy balance coefficient (CEB) in both concentric tube heat exchangers and plate heat exchangers for both parallel and counter flow arrangements.

In concentric tubing, the lowest CEB of 1.017 occurs at a parallel cold flow rate of 0.5L/min, with the highest coefficient of 1.067 at a parallel flow rate of 1.0L/min (Figure 7). Counter flow experienced a more stable CEB having a more effective energy absorbed to energy emitted ratio.

Figure 8 shows plate heat exchangers have the lowest CEB of 0.516 which occurred at a parallel cold flow rate of 3.0L/min, converging back to a stable coefficient at 2.0L/min.

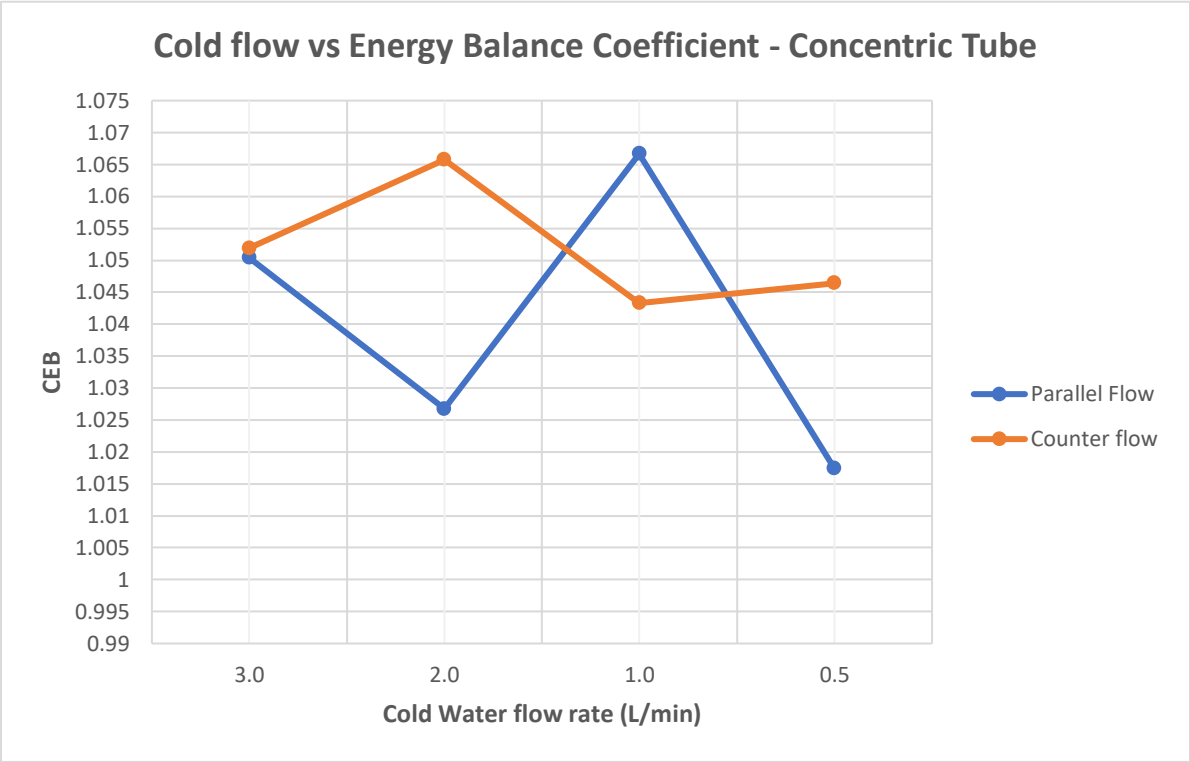

Figure 7: Cold flow rate and energy balance coefficient for concentric tube heat exchanger flows.

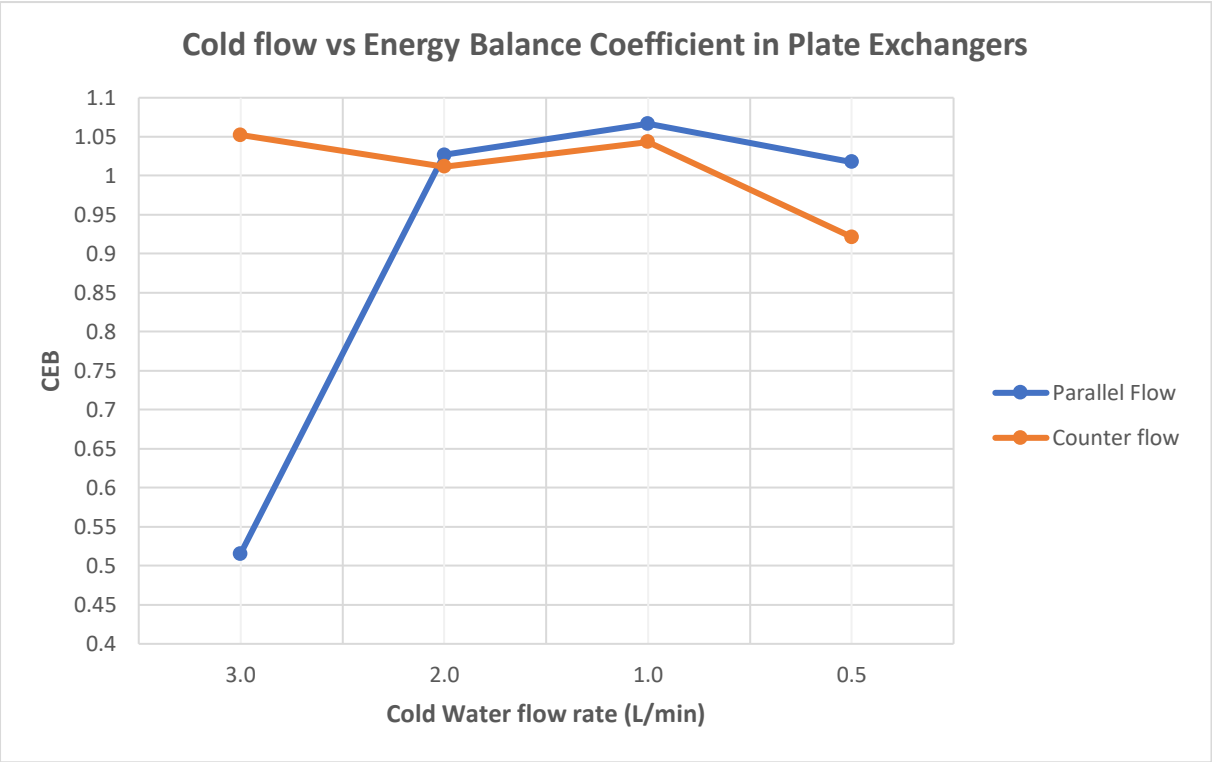

Figure 8: Cold flow rate and energy balance coefficient for plate heat exchanger flow orientations.

Due to the large initial temperature difference at fluid intake for parallel flow, a decaying heat transfer profile is imminent. The reducing temperature difference towards the outlet is unstable and unpredictable deeming it an inefficient method. As seen in Figure 6 the counter flow plate exchanger is the most efficient due to the constant temperature difference across the entire profile (Schlunder 1983). This can be further seen in test 1 with a cold flow rate of 3.0L/min. This is due to water at the same temperature running past the intake and outlet points.

The LMTD confirms this by having a larger temperature difference for counter flow arrangements in the plate heat exchanger for both flow rates. Counter flow arrangements are seen to be more stable from Figure 7&8 due to the energy absorbed to emitted ratio.

Due to the plate heat exchanger experiment being conducted across a 3 minute period, the effectiveness of each method is not outlined properly. In the TD360 manual it is specified to use exactly 20℃ cold water flow which was not done as the entering cold water was 25℃. It should also be noted that the LMTD calculation method was given inaccurately in the lab manual as it was only shown for parallel flow calculations.

4.0 Conclusion

The experimental investigation does not effectively confirm the published data regarding the effects of varying flow rate in heat exchangers. The concentric tube heat exchanger displays an inaccurate display of the published findings and does not differ between flow rates. The counter flow arrangements in the plate heat exchanger displayed a greater log mean temperature difference and a more stable temperature gradient. The counter flow plate heat exchanger with a cold flow rate of 3.0L/min displayed the largest log mean temperature difference, although not the highest heat transfer coefficient. This was deemed due to errors within the experiment such as testing time and cold water temperature.

It is recommended in further experiments to demonstrate the effects of baffles and effective length on the efficiency of shell and tube heat exchangers. The effectiveness of different arrangements could also be demonstrated through experimenting the effects of varying temperatures.

5.0 References

- Çengel, Y, Cimbala, J & Turner, R 2017, *Fundamentals of Thermal-Fluid Sciences*, 5th edn, McGraw-Hill Education, New York.
- Çengel, Y & Ghajar, A 2015, *Heat and mass transfer*, McGraw Hill, New York.
- Huang, Y 1989, "Study of Unsteady Flow in the Heat Exchanger by the Method of Characteristics", *Recent Advances in Computational Fluid Dynamics*, pp. 454-483.
- Schlunder, E 1983, *Heat exchanger design handbook*, VDI-Verlag, Dusseldorf.
- Forsberg, C 2021, *Heat transfer principles and applications*, Academic Press, London ;San Diego, CA.

6.0 Appendix

Table A1: Raw data for concentric tube heat exchanger.

Concentric Tube – Parallel Flow:

Test #	Hot Flow (deg C)	Cold Flow (deg C)	TC1 (deg C)	TC2 (deg C)	dTC (deg C)	TC3 (deg C)	TH1 (deg C)	TH2 (deg C)	dTH (deg C)	TH3 (deg C)	$\dot{Q}_e$ (W)	$\dot{Q}_a$ (W)
1	3.0	3.0	25.20	30.50	5.30	28.10	60.60	55.50	5.10	58.10	1050.25	1103.159
4	3.0	0.50	25.30	38.60	13.30	32.70	60.50	58.30	2.20	59.40	452.82	460.6875

Concentric Tube – Counter Flow:

Test #	Hot Flow (deg C)	Cold Flow (deg C)	TC1 (deg C)	TC2 (deg C)	dTC (deg C)	TC3 (deg C)	TH1 (deg C)	TH2 (deg C)	dTH (deg C)	TH3 (deg C)	$\dot{Q}_e$ (W)	$\dot{Q}_a$ (W)	C
1	3.0	3.0	25.00	30.10	5.10	27.60	59.90	55.00	4.9	57.5	1009.31	1061.70	
4	3.0	0.50	25.00	39.30	14.30	33.20	60.90	58.60	2.3	60.1	473.27	495.24	

Plate Exchanger – Parallel Flow

Test #	Hot Flow (deg C)	Cold Flow (deg C)	TC1 (deg C)	TC2 (deg C)	dTC (deg C)	TC3 (deg C)	TH1 (deg C)	TH2 (deg C)	dTH (deg C)	TH3 (deg C)	$\dot{Q}_e$ (W)	$\dot{Q}_a$ (W)	L (deg C)
1	3.0	3.0	24.9	27.5	2.6	26.2	60.6	55.5	5.1	58.05	1050.27	541.51	3
4	3.0	0.50	25.3	38.6	13.3	31.95	60.5	58.3	2.2	59.4	452.82	460.80	2

Plate Exchanger – Counter Flow:

Test #	Hot Flow (deg C)	Cold Flow (deg C)	TC1 (deg C)	TC2 (deg C)	dTC (deg C)	TC3 (deg C)	TH1 (deg C)	TH2 (deg C)	dTH (deg C)	TH3 (deg C)	$\dot{Q}_e$ (W)	$\dot{Q}_a$ (W)	L (deg C)
1	3.0	3.0	24.9	27.5	2.60	26.20	60.50	58.0	2.5	59.25	514.60	541.51	32
4	3.0	0.50	25.0	33.2	8.20	29.10	61.20	59.7	1.5	60.45	308.61	284.37	3